

Electrochemical Studies and XPS Analysis of the Surface of Zirconium-702 in Concentrated Nitric Acid With and Without Fluoride Ions

J. Jayaraj¹ · D. Nanda Gopala Krishna¹ · C. Mallika¹ · U. Kamachi Mudali²

Received: 7 February 2017 / Accepted: 13 June 2017 / Published online: 30 June 2017
© The Indian Institute of Metals - IIM 2017

Abstract Zirconium exhibited pseudo-passive behavior in fluorinated nitric acid (11.5 M HNO₃ + 0.05 M NaF) as the current density measured from the electrochemical studies was several orders higher than the value in fluoride free nitric acid. Impedance studies on zirconium sample exposed in 11.5 M HNO₃ for 240 h confirmed the formation of the passive film with high polarization resistance value and the calculated thickness of the film based on the capacitance value was about ~4.5 nm. On the other hand, in fluorinated nitric acid, the charge transfer resistance value associated with the zirconium dissolution process was dominant when compared to that of the film formation. Results of X-ray photoelectron spectroscopic investigations upheld the presence of ZrOF₂ and ZrF₄ and indicated that the protective oxide layer growth was restricted by the presence of fluoride ions.

Keywords Zirconium · Nitric acid · Fluoride · Corrosion · EIS · XPS

1 Introduction

For the dissolution of U–Pu mixed carbide spent fuel discharged from the fast breeder test reactor at Kalpakkam, 11.5 M nitric acid is used as the processing medium. Zirconium and its alloys exhibit high corrosion resistance in boiling nitric acid when compared to stainless steel, titanium and titanium alloys [1]. Zirconium grade R 60702 has been used as an evaporator material and a material for dissolver vessels in the La Hague reprocessing plant in France [2]. A zircaloy-4 mockup dissolver vessel reveals no corrosion attack when it is brought in contact with a simulated dissolver solution comprising of fission and corrosion products, in boiling 11.5 M nitric acid for 2500 h [3]. However, zircaloy-4 coupons indicate extremely high corrosion rate in boiling 11.5 M HNO₃ + 0.05 M NaF, which is the proposed processing medium for the effective dissolution of the Pu-rich, U–Pu mixed oxide fuel [4].

The dissolution behavior of zirconium was investigated by several researchers in hydrofluoric (HF) acid [5–7]. Zirconium dissolves in aqueous HF with the evolution of H₂ and formation of fluoro zirconic acid in the solution and the surface become black coloured due to the formation of hydride film [5–7]. Smith and Hill [5] studied the rate of dissolution of zirconium in HF and observed the dissolution rate to be directly proportional to un-ionized HF concentration. James et al. [6] measured the volume of H₂ evolved during the dissolution of zirconium in HF and predicted the kinetics of the reaction to follow the first order. On the other hand, Van der Wall and Whitner [8] studied the dissolution of zirconium in a mixture of HNO₃ (2–13 M) and 0.5 M HF and found out that the rate of dissolution of zirconium was first order with respect to HF. Goncalves and Munzel [9] reported that for different concentrations of HF (0.005, 0.01, 0.05 and 0.1 M) and HNO₃ (1, 3, 6 and 14 M), the

✉ J. Jayaraj
jraj@igcar.gov.in

D. Nanda Gopala Krishna
dhaipule@igcar.gov.in

C. Mallika
mallika@igcar.gov.in

U. Kamachi Mudali
kamachi@igcar.gov.in

¹ Corrosion Science and Technology Division, Metallurgy and Materials Group, Indira Gandhi Centre for Atomic Research (IGCAR), Kalpakkam 603102, India

² Materials Chemistry & Metal Fuel Cycle Group, IGCAR, Kalpakkam, India

dissolution of zircaloy-2 was proportional to HF concentration. In the mixture of HNO_3 and HF, the dissolution of zirconium occurred predominately with the evolution of NO_2 and formation of nitrous and fluoro zirconic acids [10]. Though the concentration of HNO_3 did not appear to be important for the dissolution rate of zirconium, it became vital in the production of species such as NO_2 and nitrous acid in the solution [10]. A zirconium sample exposed to a mixture of HNO_3 and HF exhibited a bright surface and thus, used as pickling medium for the surface treatment of zirconium alloys [11].

In the literature, limited information is available on the electrochemical behavior of zirconium dissolution in HF and mixture of HNO_3 and HF. In a pickling solution of 4.5 M HNO_3 + 1.1 M HF, a constant anodic current plateau was observed at stirred condition, which was attributed to the characteristic mass transfer control of the process [11]. In a solution containing 0.01 M HF in 1.2 M HNO_3 , anodic dissolution current of zirconium was measured as a function of the speed of a rotating disc electrode and the order of the reaction was found to be slightly more than one [12]. To explain the dissolution and passivation behavior, Prono et al. [13] proposed a seven-step reaction mechanism involving three adsorbed intermediates from the current–potential curves of rotating zirconium and zircaloy-4 electrodes in a pickling bath composition of 7 M HNO_3 + 0.12 M NaF.

The objective of this work is to bring insight to the corrosion behavior of commercial pure Zirconium-R 60702 (from now on referred as Zr-702) in the environments (11.5 M HNO_3 and 11.5 M HNO_3 + 0.05 M NaF) prevailing during the dissolution of spent Pu-rich nuclear fuel. Electrochemical techniques like potentiodynamic polarization, potentiostatic current transient technique, and electrochemical impedance spectroscopy experiments have been employed to understand the film properties formed on the Zr-702 sample. X-ray photoelectron spectroscopic (XPS) investigation has been carried out to analyze the chemical composition of the species present in the surface film.

2 Experimental Procedure

2.1 Materials and Test Environment

The composition analyzed by ICP-AA technique of Zr-702 material is given in Table 1. Coupons for corrosion testing

were prepared from mill annealed plates by cutting them using diamond wheel in a flowing coolant. The electrochemical and corrosion behavior of Zr-702 were evaluated in 11.5 M HNO_3 (referred as nitric) and 11.5 M HNO_3 + 0.05 M NaF (fluorinated nitric acid) solutions. The electrochemical experiments were conducted at room temperature in an aerated condition. Analytical grade reagents and double distilled water were used to prepare the test solutions.

2.2 Electrochemical Measurements

Electrochemical studies were carried out in nitric acid and fluorinated nitric acid media using a potentiostat (Autolab PGSTAT302N, The Netherlands) connected to a corrosion cell of three-electrode configuration. The Zr-702 samples (working electrode with exposed surface area of 1 cm^2) were polished by wet grinding with 1200 grit SiC paper, cleaned with ethanol, washed with distilled water and air-dried to promote reproducible surfaces. Platinum and Ag/AgCl (3 M KCl), respectively were used as counter and reference electrodes. The open circuit potential (OCP) was monitored for 2 h. The potentiodynamic polarization tests were carried out at the scanning rate of 0.166 mV s^{-1} , starting from 200 mV versus Ag/AgCl below OCP and up to 2000 mV versus Ag/AgCl. Potentiostatic current transient experiments were performed for 2 h at an anodic potential in the constant current region of the potentiodynamic polarization curve. Electrochemical impedance spectroscopic (EIS) experiments were carried out at OCP in the frequency range 0.01–100,000 Hz by superimposing an ac voltage of 10 mV amplitude and by recording 10 points per decade of frequency. In order to understand the effect of electrolyte (nitric and fluorinated nitric acid), the EIS experiments were conducted and compared for an exposed period of 2 h. However, to study the effect of exposure period on the passive film properties in nitric acid medium, EIS data were registered at the OCP values corresponding to different time periods of 2, 7.5, 15, 30, 60, 120 and 240 h. It is worth mentioning that all the steady state impedance data presented in this work has been validated using the Kramers–Kronig transforms (KKT) available in NOVA 1.1 software. On the other hand, for longer exposure periods in fluorinated nitric acid, the impedance data measured was not presented due to the non-steady state conditions provoked by severe dissolution.

Table 1 Elemental composition of zirconium (Zr-702) in weight percentage

Material	Zr	Hf	Fe	Cr	Ni	Cu
Zirconium-702 (wt%)	bal	2.4	0.06	0.05	0.005	0.005

2.3 Surface Characterization

To understand the corrosion behavior of Zr-702 samples, scanning electron microscopic (SEM) and X-ray photoelectron spectroscopic (XPS) analyses were carried out. A SNE3000M, desktop model SEM was used to observe the surface morphology of exposed samples in secondary electron mode at an accelerating voltage of 30 kV. XPS investigations were carried out using SPECS Surface Nano Analysis GmbH; Germany make spectrometer. Aluminium $K\alpha$ was used as the X-ray source at 1486.7 eV, and the anode was operated at the voltage of 13 kV with source power level at 300 W. The peak positions were compared with the standard values reported in the literature as well as the databases for identification of different elements and their oxidation states. Data were processed by SpecsLab2 software and analyzed by CasaXPS software, after correcting for background for all the peaks using Shirley approximation algorithm. The individual high resolution spectra were de-convoluted using a pseudo-voigt function with a product of Gaussian (70%) and Lorentz (30%) functions. The fitted overlay of all the individual de-convoluted spectra was similar to the recorded spectra which resulted in minimal fitting residuals. Indeed, the difference in the total area under the obtained spectra and the de-convoluted peaks were about 1.1% and the standard deviation of residual values were about 1.1 ± 0.3 , indicating the goodness of fit. Depth profile information was obtained by sputtering the specimens using an argon ion gun operating at 1 keV and 0.5 μA with a beam spot size of 0.5 mm diameter was rastered through a surface area of 60 mm². On the standard Ag layer, the sputtering rate was calculated to be about 0.0166 nm s⁻¹.

3 Results and Discussion

3.1 Time Dependence of Open Circuit Potential of Zr-702

The time dependence of OCP of Zr-702 samples in nitric acid and fluorinated nitric acid at room temperature are shown in Fig. 1a. When Zr-702 is exposed for 2 h in nitric acid, the initial OCP value of about 748 mV versus Ag/AgCl, further ennobles to reach a value of 845 mV versus Ag/AgCl. Even for a relatively longer exposure of 240 h, the OCP values recorded confirm the ennoblement behavior of Zr-702 in nitric acid as shown in Fig. 1b. For nitric acid concentration of more than 8 M, oxidizers such as nitrous acid and nitrogen dioxide will be produced due to the autocatalytic reduction of nitric acid [14]. The high oxidizing nature of the medium is attributed to the ennoblement of OCP. In fluorinated nitric acid, the initial OCP

value of about -289 mV versus Ag/AgCl, which shifts to the further active direction to a value of -366 mV versus Ag/AgCl and finally reaches -310 mV versus Ag/AgCl at the end of 2 h, is shown in Fig. 1. A similar trend of drift in OCP to lower values and finally to attain a steady state value has been reported for pure zirconium when exposed to 0.1 M NaF + 0.05 M H₂SO₄ and 0.1 M NaCl + 0.05 M H₂SO₄ [12]. Similarly, the shifting of OCP value to the active direction in fluorinated nitric acid can be due to the presence of highly electronegative and corrosive fluoride ions [12].

3.2 Potentiodynamic Polarization and Potentiostatic Current Transient Behaviors of Zr-702

The potentiodynamic polarization curves recorded for Zr-702 samples in nitric acid and fluorinated nitric acid at room temperature are shown in Fig. 2. By Tafel analysis [15], the corrosion potential (E_{corr}) and corrosion current density (I_{corr}) are obtained as shown in Table 2.

The E_{corr} values follow a similar trend as that of OCP in both nitric and fluorinated nitric acid solution. It is well known that the valve metal like Zr undergoes spontaneous passivation behavior (Fig. 2) in nitric acid [16, 17]. Passivation of Zr-702 in nitric acid is due to the formation of the ZrO₂ film, and the transpassive behavior is associated with the formation of ZrO²⁺ and O₂ evolution [16, 17]. On the other hand, in fluorinated nitric acid, for the potential above E_{corr} , the current density remains constant but several orders higher than the value in nitric acid, indicating a pseudo-passive behavior (as shown in Fig. 2). A distinctive transpassive behavior as observed in nitric acid is not found; it indicates that the O₂ evolution process may be masked when exposed to fluorinated nitric acid. The I_{corr} value of Zr-702 in fluorinated nitric is 13,333 times higher than that in nitric acid indicating the severity of corrosion due to the presence of fluoride ions.

Further to confirm the pseudo-passive behavior of Zr-702 in fluorinated nitric acid, the potentiostatic current transient behavior (Fig. 3) has been studied for 2 h and compared with nitric acid without fluoride ions. An anodic potential of 1100 and 600 mV is chosen from the constant current region of the potentiodynamic polarization curves of Zr-702, in nitric acid and fluorinated nitric acid media, respectively. The total charge density (q) corresponds to the area under the curve of current density-time (Fig. 3a), which is as high as 10.7 C cm⁻² in the fluorinated nitric acid when compared to 0.007 C cm⁻² in nitric acid. Further, the log-log plots (Fig. 3b) of current density versus time show that after the initial few seconds, slope, $m = 0$, imply corrosion process [18]. On the other hand, in nitric acid medium, $m = -1$, indicates that the formation of a ZrO₂ film is high field controlled growth [18].

Fig. 1 Time dependence of open circuit potential (OCP) of Zr-702 samples (a) in 11.5 M HNO₃ and 11.5 M HNO₃ + 0.05 M NaF for 2 h (b) in 11.5 M HNO₃ for different time periods

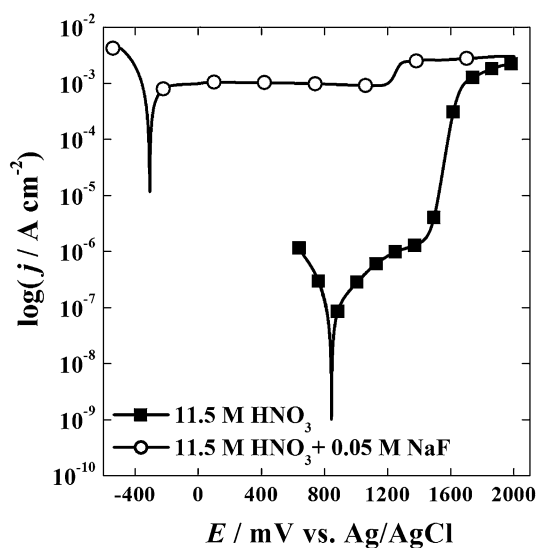
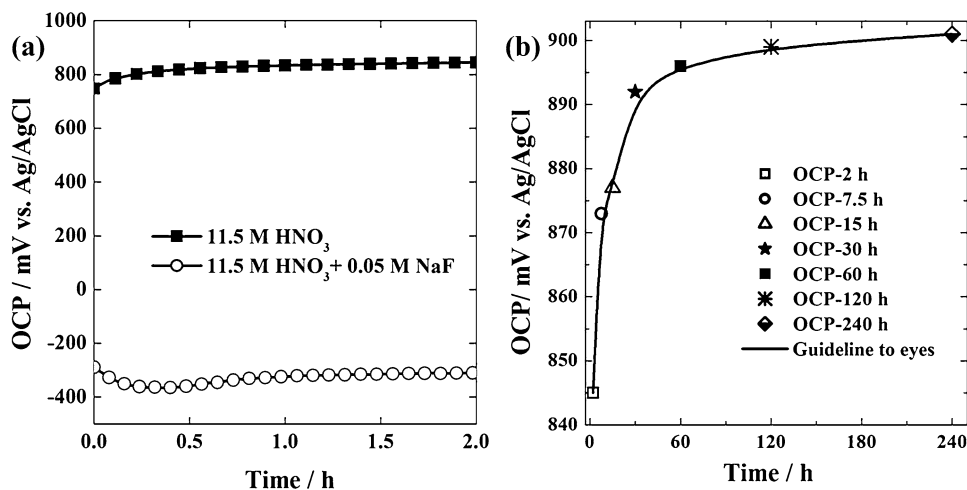
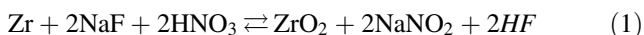


Fig. 2 Potentiodynamic polarization curves for Zr-702 samples in 11.5 M HNO₃ and 11.5 M HNO₃ + 0.05 M NaF. The scan rate used was 0.166 mV s⁻¹

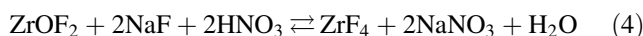
Table 2 Potentiodynamic polarization parameters for Zr-702 in 11.5 M HNO₃ and 11.5 M HNO₃ + 0.05 M NaF

Condition	E _{corr} mV versus Ag/AgCl	I _{corr} mA cm ⁻²
11.5 M HNO ₃	844	0.0003
11.5 M HNO ₃ + 0.05 M NaF	-308	4.00

In fluorinated nitric acid, due to the presence of the nitric acid and fluoride ions, the formation of ZrO₂ and dissolution is possible simultaneously according to the reactions (1) and (2).



As fluoride ion is highly electronegative in nature, it has a strong tendency to attack ZrO₂ and produce ZrF₄. Formation of ZrF₄ through the intermediate ZrOF₂ is also possible as per reactions (3) and (4).



The high I_{corr} and q values obtained from the potentiodynamic polarization and potentiostatic current transient experiments respectively can be attributed to the simultaneous formation and dissolution of the film, as explained above through Eqs. (1)–(4).

3.3 EIS Analysis of Zr-702 in Nitric Acid and Fluorinated Nitric Acid

In nitric acid medium, impedance spectra are recorded for the OCP values (Table 3) corresponding to the time periods 2, 7.5, 15, 30, 60, 120 and 240 h. The EIS results are shown as Nyquist plot (Fig. 4a, b), reveals one capacitance loop throughout the frequency range studied. The capacitance loops are incomplete, depressed semi-circles and differ distinctively depending on the exposed period. The equivalent circuit [R_s(QR_p)] shown in Fig. 4c is used for fitting all the impedance spectral data obtained in nitric acid. The % of error for each of the modeled electrical elements is within 1 to 2%, with χ² values for fitting in the range of 0.1 to 0.25, which indicates a good fit. Here, R_s is the solution resistance; Q is the constant phase element, and R_p is the polarization resistance. Instead of ideal capacitance, Q is used in the present investigation to obtain a better fit for the experimental data [19]. The impedance of Q is given as

Fig. 3 Potentiostatic polarization curves for Zr-702 samples in 11.5 M HNO₃ and 11.5 M HNO₃ + 0.05 M NaF. Potentials of 1100 and 600 mV versus Ag/AgCl were applied for 2 h, in nitric acid and fluorinated nitric acid media respectively. **a** Linear-linear plot of current density–time and **b** log-log plot of current density–time

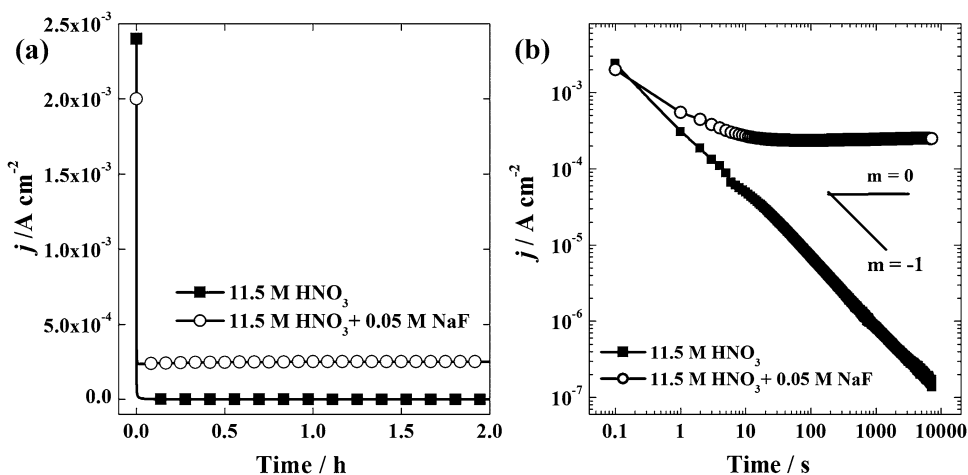
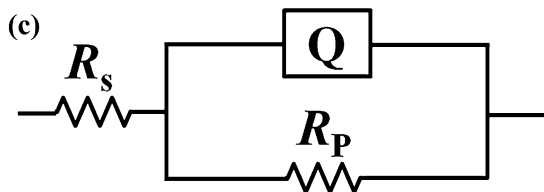
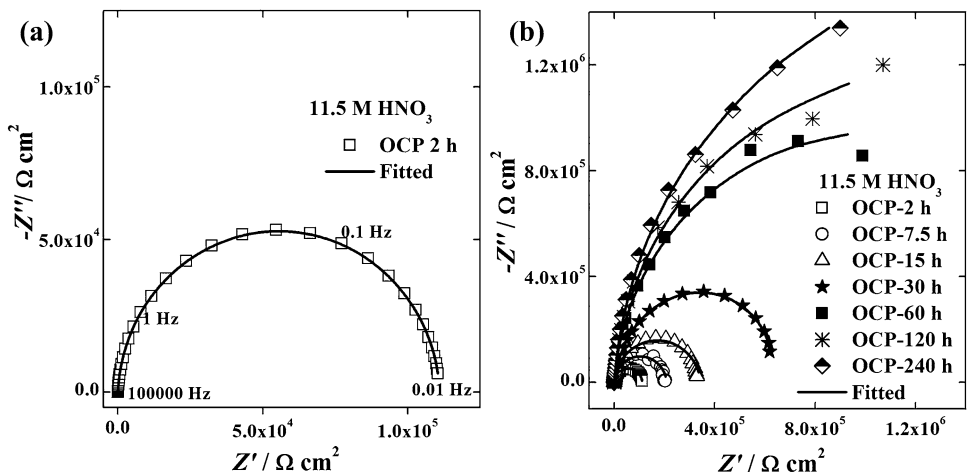


Table 3 Electrochemical impedance parameters for Zr-702 in 11.5 M HNO₃ for different exposure periods. The % of error for each of the modeled electrical elements is within 1 to 2%, with the χ^2 value for fitting is in the range of 0.1 to 0.25

Time h	OCP mV versus Ag/AgCl	R _s Ω cm ²	R _p kΩ cm ²	Y ₀ μΩ ⁻¹ S ⁿ	n	C μF cm ⁻²	d nm
2	845	1.01	111	7.35	0.98	5.78	3.83
7.5	873	1.14	208	7.32	0.97	5.10	4.34
15	877	1.46	343	7.20	0.97	5.05	4.38
30	892	1.72	694	7.10	0.97	5.00	4.43
60	896	1.12	1890	6.98	0.97	4.85	4.56
120	899	1.46	2340	6.96	0.97	4.88	4.54
240	901	1.68	3010	6.95	0.97	4.89	4.53

Fig. 4 Electrochemical impedance spectra (Nyquist plot) of Zr-702 samples in 11.5 M HNO₃ for (a) the exposure period of 2 h (b) different exposure periods (c) [R_s(QR_p)] equivalent circuit used for fitting the data obtained in 11.5 M HNO₃



$$Z_Q = Y_0^{-1}(j\omega)^{-n} \quad (5)$$

where, Y_0 is a constant with the unit $\Omega^{-1} S^n$, n is the power index value of Q , ω is the angular frequency and j is the imaginary number equal to $\sqrt{-1}$. The conversion of Y_0 to capacitance (C) value is calculated using the following Brug's equation as explained elsewhere [20, 21]:

$$C = [Y_0(R_S^{-1} + R_P^{-1})^{n-1}]^{1/n} \quad (6)$$

Q can be considered as a general element with it representing a capacitance when $n = 1$, a resistance when $n = 0$ and an inductance when $n = -1$. Here we use it to represent the electrode–electrolyte interface, which appears as a non-ideal capacitor as the obtained exponent n values is slightly lower than 1 (Table 3) and the calculated C values correspond to the capacitance of the passive film. As the exposure period is increased, the calculated C values show neither increasing nor decreasing trend, but remain almost constant. The thickness (d) of the passive film that is formed on Zr-702, when exposed to nitric acid for different exposure period is calculated by using Eq. (7)

$$d = \frac{\varepsilon\varepsilon_0}{C} \quad (7)$$

where, ε is the dielectric constant of the passive film (ε for ZrO_2 is 25), $\varepsilon_0 = 8.854 \times 10^{-14} \text{ F cm}^{-1}$ is the permittivity of free space charge and C is the capacitance of the passive film obtained from EIS (Table 3). From these results, it is clear that the capacitance and thickness of the passive film have not changed much, and it can be due to the fact that the film defects are repaired or reduced over time. As the film nature improves over time, the polarization resistance R_P increases indicating the high stability of the film that is formed in nitric acid. The stability of the passive film is attributed to the low diffusion of ionic species and/or low charge transfer and their accumulation across the film-solution interface [19].

The impedance spectrum obtained for Zr-702 in fluorinated nitric acid at the OCP value corresponding to 2 h is shown as Nyquist plot in Fig. 5a. The experimental data shows one high frequency loop corresponding to the film, one inductive loop and a capacitive loop at mid frequencies and one inductive loop at low frequencies. The equivalent circuit $[RS((QR)[L1R1][C1R3][L2R2])]$ shown in Fig. 5b has been used for fitting the EIS data in fluorinated condition. Inductive loops are observed for electrochemical systems bringing about debates in the literature on whether it should be called inductance or pseudo inductance or negative capacitance [22, 23]. The inductance does not arise from magnetic properties of the film but rather due to the electrochemical reactions with the formation of

intermediate adsorbed species and their relaxation [22, 23]. Whenever inductive loop appears in the spectra, it can also be modeled using a pair of capacitance and resistance, but with negative values [22, 24]. Thus, the equivalent circuit $[R_S((QR)[C_1R_1][C_2R_2][C_3R_3])]$ shown in Fig. 5c has also been used for fitting the EIS data in fluorinated condition. While fitting the impedance data, C_1R_1 and C_3R_3 of the equivalent circuit (Fig. 5c) are allowed to have negative values to represent the inductance [22, 24]. The fitted values are given in Tables 4 and 5 for $[R_S((QR)[L1R1][C1R3][L2R2])]$ and $[R_S((QR)[C1R1][C2R2][C3R3])]$, respectively, and the % of error for each of the modeled electrical elements is within 1 to 10%, with the χ^2 value of about 0.457 for both the circuits. Inductive loops are predicted [25] and observed in actual experimental data of electrochemical reactions such as Ta or Ti dissolving in HF [24, 26]. Zr, as a valve metal, is similar to Ti and Ta, and thus the appearance of the inductive loop in EIS data is similar to what is reported in the literature [24, 26]. The two inductance loops obtained (Fig. 5a) can be attributed to relaxation of absorbed species such as $ZrOF_2$ and ZrF_4 .

For the impedance spectra (Fig. 5a), when the $[R_S((QR)[L1R1][C1R3][L2R2])]$ circuit is used, the polarization resistance (R_P) is given by $\lim_{\omega \rightarrow 0} Z_F$, and

$$\frac{1}{R_P} = \frac{1}{R} + \frac{1}{R_1} + \frac{1}{R_2} \quad (8)$$

while, the charge transfer resistance (R_{ct}) is given by $\lim_{\omega \rightarrow \infty} Z_F$, and

$$\frac{1}{R_{ct}} = \frac{1}{R} + \frac{1}{R_3} \quad (9)$$

where Z_F is the faradaic impedance [27–29].

On the other hand, when the $[R_S((QR)[C1R1][C2R2][C3R3])]$ circuit is used, the R_P is given by $\lim_{\omega \rightarrow 0} Z_F$, and

$$\frac{1}{R_P} = \frac{1}{R} \quad (10)$$

while, the R_{ct} is given by $\lim_{\omega \rightarrow \infty} Z_F$, and

$$\frac{1}{R_{ct}} = \frac{1}{R} + \frac{1}{R_1} + \frac{1}{R_2} + \frac{1}{R_3} \quad (11)$$

where Z_F is the faradaic impedance [27–29]. At zero frequency limit, capacitance acts as an open circuit and inductance offers zero impedance, viz. it acts as a short circuit. On the other hand, at infinite frequency limit, capacitance offers zero impedance while inductance behaves as an open circuit. Thus, the resistance in series with capacitance can be neglected while calculating the polarization resistance, and the resistance in series with inductance can be neglected while calculating the charge

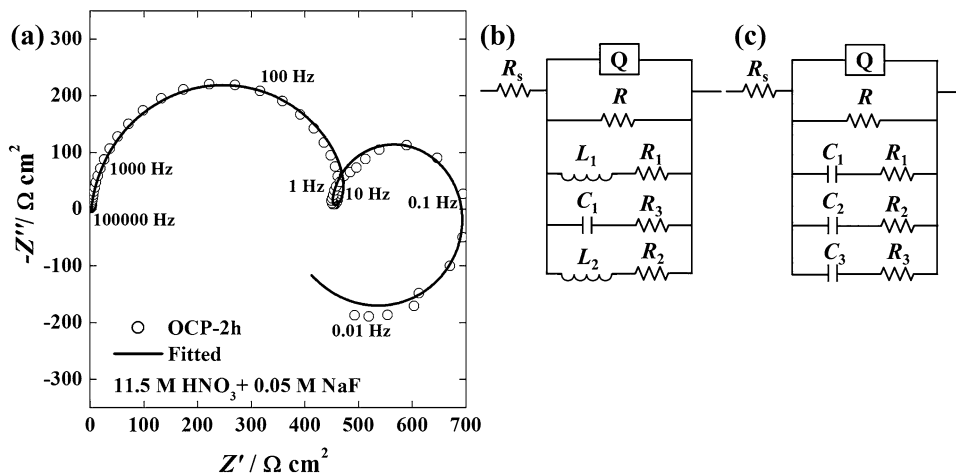


Fig. 5 a Electrochemical impedance spectra (Nyquist plot) of Zr-702 samples in 11.5 M HNO₃ + 0.05 M NaF for the exposure period of 2 h (b–c) equivalent circuits used for fitting the data shown in Fig. 5a, b [R_S((QR)[L₁R₁][C₁R₃][L₂R₂])] and (c) [R_S((QR)[C₁R₁][C₂R₂][C₃R₃])]

Table 4 Electrochemical impedance parameters obtained by fitting using the circuit [R_S((QR)[L₁R₁][C₁R₃][L₂R₂])] shown in Fig. 5c for Zr-702 in 11.5 M HNO₃ + 0.05 M NaF for the exposure period of 2 h. The % of error for each of the modeled electrical elements is within 1 to 10%, with the χ² value for fitting is about 0.457

R _S Ω cm ²	Y ₀ μΩ ⁻¹ S ⁿ	n	R Ω cm ²	L ₁ H cm ²	R ₁ Ω cm ²	L ₂ H cm ²	R ₂ Ω cm ²	C ₁ mF cm ⁻²	R ₃ Ω cm ²	R _P Ω cm ²	R _{ct} Ω cm ²
1.89	3.79	0.93	970	90	5000	7300	666	1.0	1000	366	492

Table 5 Electrochemical impedance parameters obtained by fitting using the circuit [R_S((QR)[C₁R₁][C₂R₂][C₃R₃])] shown in Fig. 5b for Zr-702 in 11.5 M HNO₃ + 0.05 M NaF for the exposure period of 2 h. The % of error for each of the modeled electrical elements is within 1 to 10%, with the χ² value for fitting is about 0.457

R _S Ω cm ²	Y ₀ μΩ ⁻¹ S ⁿ	n	R Ω cm ²	C ₁ mF cm ⁻²	R ₁ Ω cm ²	C ₂ mF cm ⁻²	R ₂ Ω cm ²	C ₃ mF cm ⁻²	R ₃ Ω cm ²	R _P Ω cm ²	R _{ct} Ω cm ²
1.89	3.79	0.93	366	-0.0036	-5000	-16.5	-666	1.0	1000	366	492

transfer resistance. The above are the definitions employed for R_P and R_{ct} in this study and it is worth noting that in some reports, both have been used interchangeably [30]. The fitting and the calculated R_P and R_{ct} values by using both the circuits yield same value as shown in Tables 4 and 5, suggesting that both the circuits has to be used to model the impedance spectra of Zr-702 in fluorinated nitric acid. The calculated R_{ct} is higher than the R_P value (Tables 4, 5) for Zr-702 in fluorinated nitric acid indicating that the R_{ct} associated with the zirconium dissolution process as ZrOF₂ and ZrF₄ (as given in Eqs. 2–4) is dominant when compared to that of the ZrO₂ film formation. Further, the obtained R_P value in fluorinated nitric is found to be much lower than the respective value in solution without fluoride ion. The lower R_P value in fluorinated nitric acid can be attributed to the formation of un-protective ZrO₂ film. Also the obtained n value is lower in fluoride solution, indicating that the surface can be rougher as shown in the following SEM analysis, Sect. 3.4.

3.4 SEM Analysis of Zr-702 in Nitric Acid and Fluorinated Nitric Acid

SEM investigation reveals un-attacked and smooth surface morphology as shown in Fig. 6a, b for the Zr-702 samples exposed to nitric acid for 240 h at room temperature. The line marks appearing in the Fig. 6a, b are due to polishing that has been carried out before the corrosion experiments. On the other hand, uniformly attacked and relatively roughened morphology (as shown in Fig. 6c) and the presence of micro-pits at higher magnification (Fig. 6d) are observed for the Zr-702 samples exposed to fluorinated nitric acid for 2 h.

3.5 XPS Results for Zr702 in Nitric and Fluorinated Nitric Acid

XPS analysis has been performed to find out the chemical states of the films formed on the surface of Zr-702 samples

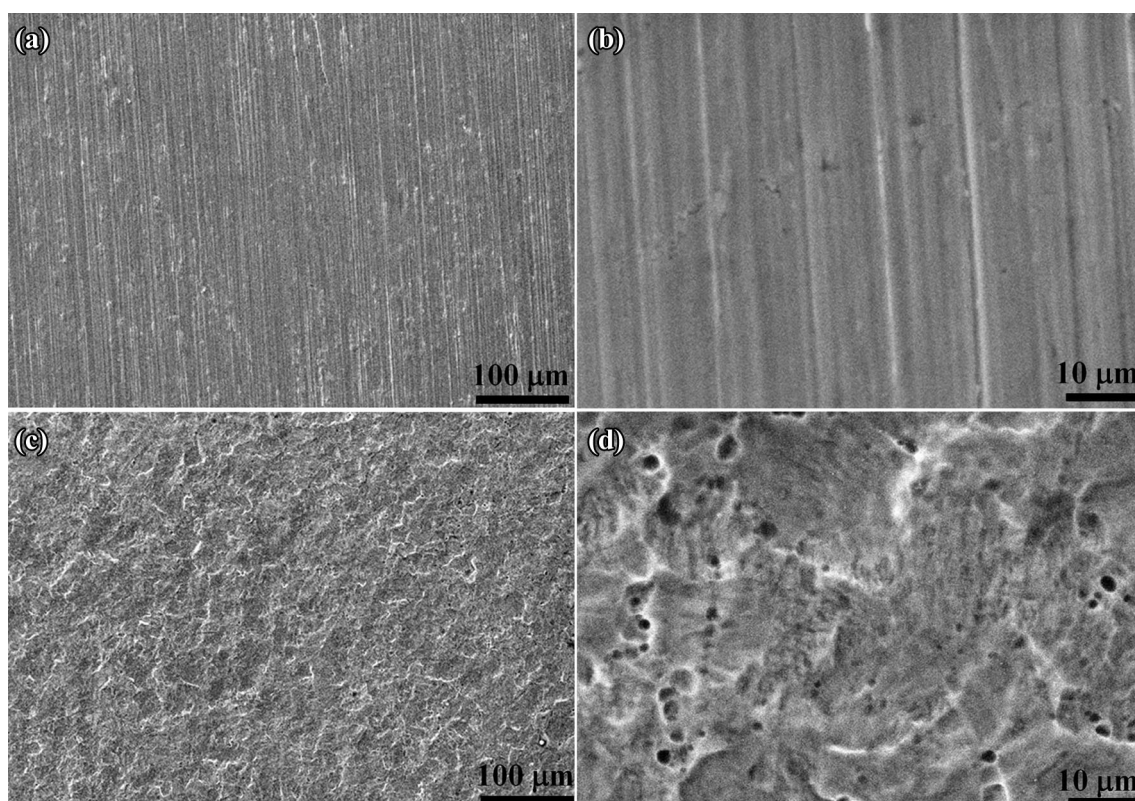


Fig. 6 SEM morphology of Zr-702 sample after exposed to (a–b) 11.5 M HNO₃ for 240 h (c–d) 11.5 M HNO₃ + 0.05 M NaF for 2 h

exposed to air, nitric acid for 240 h and fluorinated nitric acid for 2 h. High resolution scans corresponding to Zr 3d_{5/2} and Zr 3d_{3/2} spectra for the as-received conditions of Zr-702 samples exposed to air (native film), nitric acid (passive film) and fluorinated nitric acid, respectively are shown in Fig. 7.

The Zr 3d spectra shown in Fig. 7 are fitted with doublet peaks of 3d_{5/2} and 3d_{3/2} arising due to the angular momentum spin–orbit coupling of the electrons in the energy level. The energy difference between the doublets is kept constant at 2.4 eV and the intensity ratio of the individual peaks of the doublets is maintained at a ratio of 3:2 following the electron occupational probabilities of the individual states governed by quantum mechanical selection rules. The de-convoluted high resolution spectrum in the Zr 3d region of native film (Fig. 7a) reveals five sets of doublet peaks corresponding to the oxidation states Zr⁴⁺ (ZrO₂), Zr³⁺, Zr²⁺, Zr¹⁺ and metallic state of Zr to their respective binding energies shown in Table 6 [31]. In contrast, for the passive film condition, only one doublet peak of Zr 3d corresponding to the oxidation state Zr⁴⁺ (ZrO₂) is observed as shown in Fig. 7b to the corresponding binding energies shown in Table 6 [31]. It is worth mentioning that a small shift in the peaks towards the higher binding energy side for all the oxides of zirconium peaks is observed which can be attributed to the

charging effect of the insulating nature of zirconium oxides. For the native and passive film, the shift observed is higher, about 1.4 and 1.6 eV, respectively, with respect to the standard C 1 s (284.8 eV) which is considered for charge correction. For the sample exposed to fluorinated nitric acid, the Zr 3d and F 1s spectra are observed as shown in Fig. 7c, d, respectively. The high resolution of the Zr 3d region after de-convolution reveals the presence of four doublets indicating that zirconium exists in four different chemical environments corresponding to the binding energies of ZrO₂, Zr-metallic, ZrOF₂ and ZrF₄ as shown in Fig. 7c [31–33]. The F 1s region (Fig. 7d) shows a single narrow peak at 686.8 eV indicating F-Zr bonding indicating the presence of ZrOF₂ and ZrF₄. The area under the deconvoluted peaks gives the concentrations of each state, after correcting for the sensitivity factor of the respective elements. XPS results shown in Table 6 confirm that the surface state of the sample exposed to nitric acid is 100% of ZrO₂ (Zr⁴⁺), and metallic peaks are absent. In contrast, about 13.3% of Zr in metallic states is present together with the different concentration of oxides of Zr as shown in Table 6, for the as-polished condition of Zr-702 sample. From Table 6, it is found that apart from the oxide and metallic states of Zr, the total concentration of Zr-fluoride states (ZrOF₂ and ZrF₄) on the surface is about 22.8% for the sample

Fig. 7 XPS spectra of Zr 3d for Zr-702 sample surface exposed to (a) air (b) 11.5 M HNO₃ at room temperature for 240 h (c–d) 11.5 M HNO₃ + 0.05 M NaF for 2 h, (d) F 1s spectra

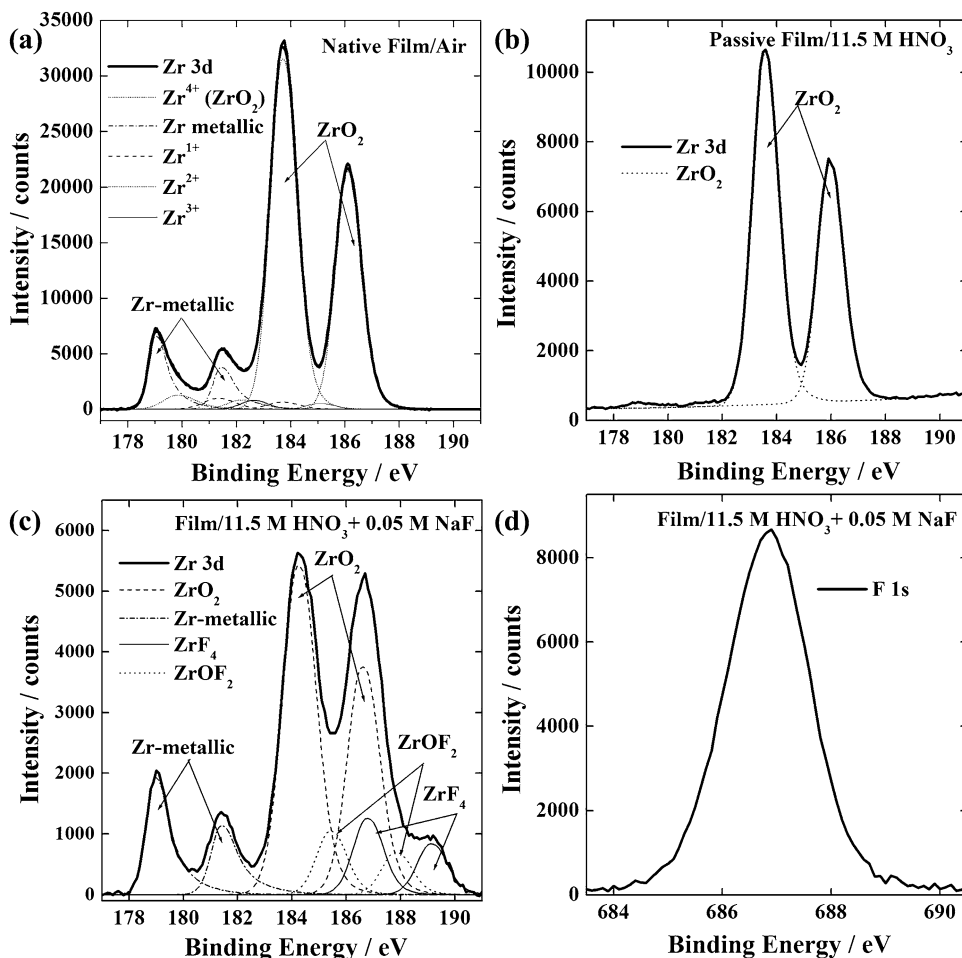


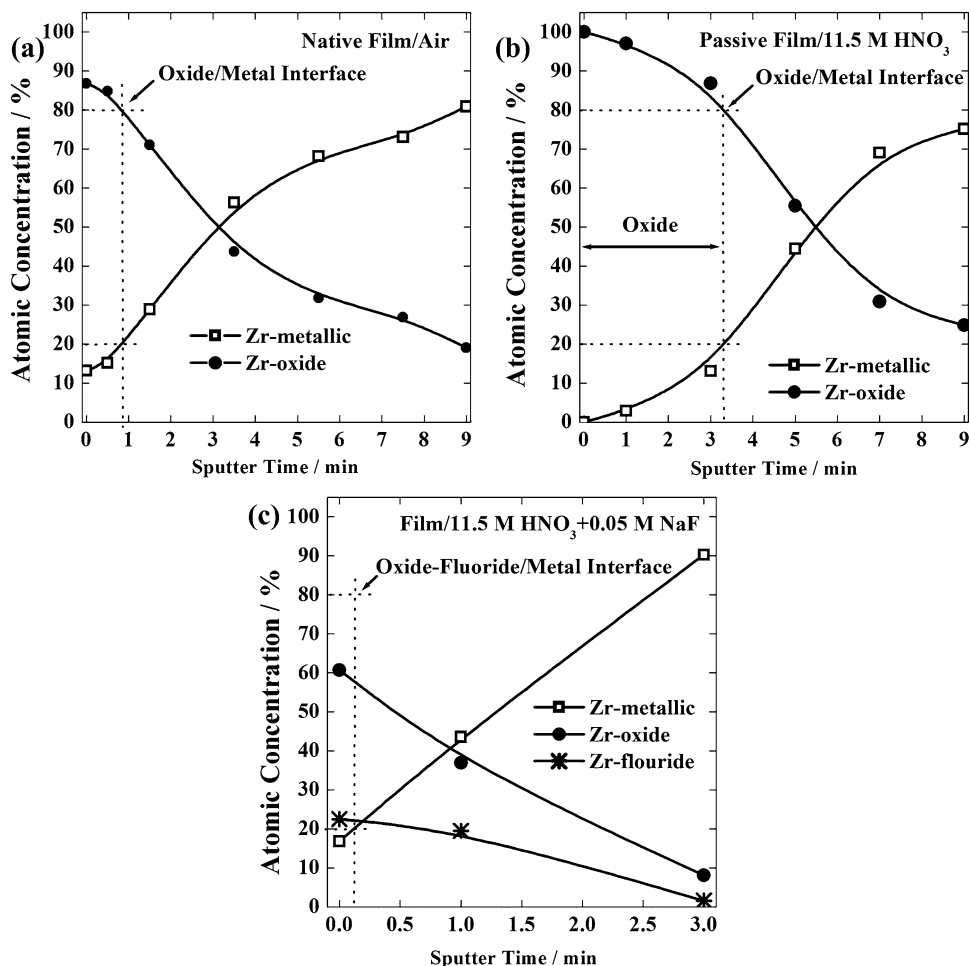
Table 6 Binding energy values and concentrations of the oxide, metallic and fluoride states of Zr present in the surface of native film formed in air; passive film formed in 11.5 M HNO₃ and the film formed in 11.5 M HNO₃ + 0.05 M NaF of Zr-702 sample

Chemical/oxidation state	Binding energy (eV)			Atomic concentration (%)		
	Native film (Air)	Passive film (HNO ₃)	Film (HNO ₃ + NaF)	Native film (Air)	Passive film (HNO ₃)	Film (HNO ₃ + NaF)
ZrO ₂ (Zr ⁴⁺)	183.7; 186.1	183.6; 186.0	184.2; 186.6	77.6	100.0	60.1
Zr-oxide (Zr ³⁺)	182.6; 185.0	–	–	2.1	–	–
Zr-oxide (Zr ²⁺)	181.3; 183.7	–	–	2.9	–	–
Zr-oxide (Zr ¹⁺)	180.2; 182.6	–	–	4.1	–	–
Zr-metal (Zr ⁰)	179.0; 181.4	–	179.0; 181.4	13.3	–	17.1
ZrOF ₂ (Zr ⁴⁺)	–	–	185.4; 187.8	–	–	10.4
ZrF ₄ (Zr ⁴⁺)	–	–	186.8; 189.2	–	–	12.4

exposed to fluorinated nitric acid. The concentration analysis of the different chemical states of Zr clearly indicates that the sample exposed to nitric acid is passivated and it is different when compared to the native film. The incorporation of F⁻ ions into the protective film and the presence of significant amount of ZrOF₂ and ZrF₄

indicate that the fluoride ions are responsible for the breakdown of the film and severe corrosion of Zr-702 when exposed to fluorinated nitric acid. To estimate the thickness of the film, the depth profile of atomic concentrations of different states with respect to sputtering time for the samples exposed to air, nitric and fluorinated

Fig. 8 Atomic concentrations of oxide, fluoride and metallic species of Zr as a function of sputtering time obtained from the XPS depth profiling of Zr-702 sample surface exposed to (a) air, (b) 11.5 M HNO₃ at room temperature for 240 h (c) 11.5 M HNO₃ + 0.05 M NaF at room temperature for 2 h; sputtering time 0 s represents the as-received condition



nitric acid are shown in Fig. 8a, b, c, respectively. The oxide/metal interface region (marked in Fig. 8) is considered to have the metallic concentration of 20% and oxide concentration of 80%, i.e. the ratio of oxide to metal is 4 [34]. Thus, the region from the outer surface to the oxide/metal interface is assumed as the oxide film. For the sample exposed to fluorinated nitric acid, the film interface (marked in Fig. 8c) is assumed to have the metallic concentration of 20% and the sum of the concentrations of oxide and fluoride as 80%, i.e. the ratio of oxide-fluoride to metal is 4. The native film thickness formed in air is estimated to be about ≈ 0.84 nm and whereas the passive film formed in nitric acid during immersion for 240 h is about ≈ 3.4 nm thick, indicating the formation of protective ZrO₂ film. In fluorinated nitric acid, from XPS depth profile the film thickness is estimated to be about ≈ 0.11 nm, which is approximately 31 times thinner than that of the film formed in nitric acid. The lower film thickness value indicates that the protective oxide layer growth is restricted due to the formation of ZrOF₂ and ZrF₄ in the fluorinated nitric acid medium.

4 Conclusion

The effect of fluoride ion on the electrochemical behavior of zirconium was studied in the concentrated nitric acid medium. Zirconium exhibited pseudo-passive behavior in fluorinated nitric acid as the current density measured from the electrochemical studies was several orders higher than the value in fluoride free nitric acid. Impedance studies on zirconium sample exposed to 11.5 M HNO₃ for 240 h confirmed the formation of the passive film with high polarization resistance value and the calculated thickness of the film based on the capacitance value was about ~ 4.5 nm. In solutions with fluoride ions, the polarization and charge transfer resistances were lower compared to the respective values in solutions without fluoride ions. In fluorinated nitric acid, the charge transfer resistance was associated with the zirconium dissolution process as ZrOF₂ and ZrF₄ and it was dominant when compared to that of the ZrO₂ film formation. XPS investigations confirmed the presence of ZrOF₂ and ZrF₄ and correlated to the electrochemical behavior of zirconium in fluorinated nitric acid.

References

1. Baldev Raj and Kamachi Mudali U, *Prog Nucl Energ* **48** (2006) 283.
2. Bernard C, Mourox J P, Decours J, Demay R and Simonnet J, Proc Int Conf on Fuel Reprocessing and Waste Management-RECOD 91, Sendai, Japan (1991) p 570.
3. Jayaraj J, Thyagarajan K, Mallika C and Kamachi Mudali U, *Nucl Technol* **191** (2015) 58.
4. Jayaraj J, Krishnaveni P, Nanda Gopala Krishna D, Mallika C and Kamachi Mudali U, *J Nucl Mater* **473** (2016) 157.
5. Smith T and Hill G R, *J Electrochem Soc* **105** (1958) 117.
6. James W J, Custead W G and Straumanis M E, *J Phys Chem* **64** (1960) 286.
7. Straumanis M E, James W J and Custead W C, *J Electrochem Soc* **107** (1960) 502.
8. Van der Wall E M and Whitener E M, *Ind Eng Chem* **51** (1959) 51.
9. Goncalves Z and Munzel H, *J Nucl Mater* **170** (1990) 261.
10. Klein R, *Corrosion* **53** (1997) 327.
11. Sutter E M M, Hlawka F and Cornet A, *Corrosion* **46** (1990) 537.
12. Meyer R E, *J Electrochem Soc* **112** (1965) 684.
13. Prono J, Jaszay T, Caprani A and Frayret J P, *J Appl Electrochem* **25** (1995) 1031.
14. Fauvet P, Balbaud F, Robin R, Taran Q T, Mugnier A and Espinoux D, *J Nucl Mater* **375** (2008) 52.
15. Fontana M G, *Corrosion Engineering*, Tata McGraw-Hill Education Private Limited, Delhi (2005).
16. Ravi Shankar A and Kamachi Mudali U, *Trans Indian Inst Metals* **62** (2009) 545.
17. Kajimura H and Nagano H, *Corros Sci* **31** (1990) 261.
18. Lohrengel M M, *Mater Sci Eng R* **11** (1993) 243.
19. Kelly R G, Scully J R, Shoesmith D W, Buchheit R G, *Electrochemical Techniques in Corrosion Science and Engineering*, Marcel Dekker Inc., New York (2003).
20. Brug G J, Van Den Eeden A L G, Rehbach M S and Sluyters J H, *J Electroanal Chem* **176** (1984) 275.
21. Torres P C, Mesquita T J, Devos O, Tribollet B, Roche V and Nogueira R P, *Electrochim Acta* **72** (2012) 172.
22. Franceschetti D R and Macdonald J R, *J Electroanal Chem* **82** (1977) 271.
23. Torres P C, Keddum M and Nogueira R P, *Electrochim Acta* **54** (2008) 518.
24. Fasmin F, Praveen B V S and Ramanathan S, *J Electrochem Soc* **162** (2015) H604.
25. Armstrong R D and Edmonson K, *Electrochim Acta* **18** (1973) 937.
26. Sapra S, Li H, Wang Z and Suni I I, *J Electrochem Soc* **152** (2005) B193.
27. Diard J P, Gorreot B L and Montella C, *J Electroanal Chem* **432** (1997) 27.
28. Harrington D A, *J Electroanal Chem* **737** (2015) 30.
29. Harrington D A, *J Electroanal Chem* **449** (1998) 9.
30. He Z and Mansfeld F, *Energ Environ Sci* **2** (2009) 141.
31. Morant C, Sanz J M, Galan L, Soriano L and Rueda F, *Surf Sci* **218** (1989) 331.
32. Bosman H J M, Pijpers A P and Jaspers A W M A, *J Catal* **161** (1996) 551.
33. Sleigh C, Pijpers A P, Jaspers A, Coussens B and Meier R J, *J Electron Spectrosc Relat Phenom* **77** (1996) 41.
34. Jayaraj J, Ravishankar A and Kamachi Mudali U, *Electrochim Acta* **85** (2012) 210.